Inorg. Chem. 2006, 45, 6851–6859

Inorganic Chemistry Article

Optimizing Small Molecule Activation and Cleavage in Three-Coordinate M[N(R)Ar]$_3$ Complexes

Gemma J. Christian,[†] Robert Stranger,*[,†] and Brian F. Yates[‡]

Department of Chemistry, Faculty of Science, Australian National University, Canberra, ACT 0200, Australia, and School of Chemistry, University of Tasmania, Private Bag 75, Hobart, TAS 7001, Australia

Received October 14, 2005

The sterically hindered, three-coordinate metal systems M[N(R)Ar]$_3$ (R = ^{t}Bu, ^{i}Pr; Ar = 3,5-$C_6H_3Me_2$) are known to bind and activate a number of fundamental diatomic molecules via a [Ar(R)N]$_3$M–L–L–M[N(R)Ar]$_3$ dimer intermediate. To predict which metals are most suitable for activating and cleaving small molecules such as N_2, NO, CO, and CN^-, the M–L bond energies in the L–M(NH_2)$_3$ (L = O, N, C) model complexes were calculated for a wide range of metals, oxidation states, and d^n (n = 2–6) configurations. The strongest M–O, M–N, and M–C bonds occurred for the d^2, d^3, and d^4 metals, respectively, and for these d^n configurations, the M–C and M–O bonds were calculated to be stronger than the M–N bonds. For isoelectronic metals, the bond strengths were found to increase both down a group and to the left of a period. Both the calculated N–N bond lengths and activation barriers for N_2 bond cleavage in the (H_2N)$_3$M–N–N–M(NH_2)$_3$ intermediate dimers were shown to follow the trends in the M–N bond energies. The three-coordinate complexes of Ta^{II}, W^{III}, and Nb^{II} are predicted to deliver more favorable N_2 cleavage reactions than the experimentally known Mo^{III} system and the Re^{III}Ta^{III} dimer, [Ar(R)N]$_3$-Re–CO–Ta[N(R)Ar]$_3$, is thermodynamically best suited for cleaving CO.

Introduction

Dinuclear metal complexes (Figure 1) based on sterically hindered three-coordinate transition metal complexes of the type M[N(R)Ar]$_3$, where R is a bulky organic substituent such as ^{t}Bu or ^{i}Pr, hold great promise synthetically for the activation and scission of small multiply bonded molecules.[1,2] Since the initial work by Laplaza and Cummins on the reductive cleavage of N_2 by the three-coordinate complex Mo[N(R)Ar]$_3$ (R = ^{t}Bu, Ar = 3,5-$C_6H_3Me_2$),[3−5] more recent studies have shown that the class of sterically hindered three-coordinate metal complexes are extraordinarily versatile, capable of binding and activating a variety of small molecules, including N_2, NO,[5] N_2O,[5] CO,[6,7] SO_2,[8] and NCO^-,[9] and other chalcogen-containing compounds, such as Se_2Ph_2 and $OSMe_2$.[8] A variety of L−M[N(R)Ar]$_3$ complexes have also been prepared which include L = NO,[5] NCO^-,[9] CO,[6,7] CN^-,[10] and PO.[11] Furthermore, these complexes offer previously unavailable synthetic routes to novel metal−element multiple bonds. To date, terminal nitride, phosphide, carbide, oxide, sulfide, selenide, and telluride species have been

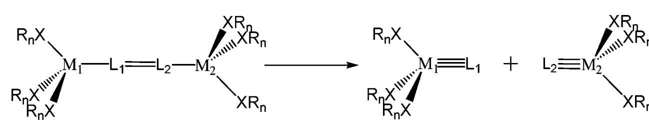

Figure 1. $L_1{\equiv}L_2$ cleavage reaction.

* To whom correspondence should be addressed. E-mail: rob.stranger@anu.edu.au.
[†] Australian National University.
[‡] University of Tasmania.

(1) Fryzuk, M. D.; Johnson, S. A. *Coord. Chem. Rev.* **2000**, *200−202*, 379−409.
(2) Howard, J. B.; Rees, D. C. *Chem. Rev.* **1996**, *96*, 2965−2982.
(3) Laplaza, C. E.; Cummins, C. C. *Science* **1995**, *268*, 861−863.
(4) Laplaza, C. E.; Johnson, M. J. A.; Peters, J. C.; Odom, A. L.; Kim, E.; Cummins, C. C.; George, G. N.; Pickering, I. J. *J. Am. Chem. Soc.* **1996**, *118*, 8623−8638.
(5) Laplaza, C. E.; Odom, A. L.; Davis, W. M.; Cummins, C. C.; Protasiewicz, J. D. *J. Am. Chem. Soc.* **1995**, *117*, 4999−5000.
(6) Peters, J. C.; Odom, A. L.; Cummins, C. C. *Chem. Commun.* **1997** No. 20, 1995−1996.
(7) Greco, J. B.; Peters, J. C.; Baker, T. A.; Davis, W. M.; Cummins, C. C.; Wu, G. *J. Am. Chem. Soc.* **2001**, *123*, 5003−5013.
(8) Johnson, A. R.; Davis, W. M.; Cummins, C. C.; Serron, S.; Nolan, S. P.; Musaev, D. G.; Morokuma, K. *J. Am. Chem. Soc.* **1998**, *120*, 2071−2085.
(9) Fickes, M. G.; Odom, A. L.; Cummins, C. C. *Chem. Commun.* **1997** No. 20, 1993−1994.
(10) Peters, J. C.; Baraldo, L. M.; Baker, T. A.; Johnson, A. R.; Cummins, C. C. *J. Organomet. Chem.* **1999**, *591*, 24−35.
(11) Johnson, M. J. A.; Odom, A. L.; Cummins, C. C. *Chem. Commun.* **1997**, No. 16, 1523−1524.

10.1021/ic051778u CCC: $33.50

Published on Web 07/19/2006

prepared by reacting the three-coordinate metal complex with the appropriate elemental source.[12]

The steric bulk of the N(R)Ar ancillary ligands is essential in stabilizing the coordinatively unsaturated, three-coordinate metal complex, preventing dimerization to form the metal−metal-bonded species $[Ar(R)N]_3M{\equiv}M[N(R)Ar]_3$. Furthermore, tuning the size of the R groups allows the possibility of accommodating small molecules other than N_2. Interestingly, when R = ^{i}Pr, the reaction with N_2 results in the single-atom-bridged complex $[Ar(R)N]_3Mo{-}N{-}Mo[N(R)Ar]_3$ and not the nitride product $[Ar(R)N]_3Mo{-}N$.[13] This is thought to occur via reaction of the nitride product with unreacted $[Ar(R)N]_3Mo$. For the R = ^{t}Bu system, the more bulky ^{t}Bu group prevents the formation of the single-atom-bridged species. The degree of activation can also be controlled electronically by changing one or both metal ions. For instance, whereas the dimolybdenum(III) complex $[Ar(R)N]_3Mo$-(μ-N_2)$Mo[N(R)Ar]_3$ cleaves dinitrogen, the corresponding Mo(III)Nb(III) dimer $[Ar(R)N]_3Mo(\mu\text{-}N_2)Nb[N(R)Ar]_3$ activates N_2 but only cleaves N_2 in the presence of a reducing agent.[14] The existence of heteronuclear species such as $[Ar(R)N]_3Mo(\mu\text{-}N_2)Nb[N(R)Ar]_3$ highlights the potential for tuning the metal centers to optimize the small molecule activation, particularly for unsymmetrical molecules such as NO, CO, and CN^-, where the bridging donor atoms are different.

The ease with which the $Mo[N(R)Ar]_3$ (R=^{t}Bu, Ar = 3,5-$C_6H_3Me_2$) complex binds and cleaves N_2 makes it and related complexes potentially very useful in the area of N_2 activation. On the basis of several experimental[4,15,16] and theoretical[17−19] studies, the mechanism of the N_2 cleavage reaction is now well understood. In addition, the selected N−N bond cleavage in N_2O has been investigated.[5,20,21] The versatility with which these systems bind small molecules, and the relative ease with which they activate and cleave N_2 and N_2O, suggests that with a careful choice of metals they could be useful in activating and cleaving other small multiply bonded molecules. Accordingly, we have embarked on a course of investigation to extend the work on N_2 by optimizing the $M[N(R)Ar]_3$ system for the activation and cleavage of other small molecules. In this paper, we set out and test a computational strategy, described below, to deal with these systems and their optimization efficiently.

Strategy

There are several requirements for a system to cleave a small diatomic molecule such as N_2. The system must have metals that are capable of binding the desired small molecule and providing the required number of electrons to reductively cleave the multiple bond. There must also be a strong thermodynamic driving force for the cleavage to occur and the activation barrier involving the cleavage step must be thermally accessible.

In our previous work,[22] the trend in N_2 activation was investigated by performing calculations on the model intermediate dimer, $[R_nX]_3M{-}N{-}[XR_n]_3$ for different metals, M, and ancillary ligands, R_nX. This study found that metals with a d^3 configuration gave the best activation and cleavage of N_2, whereas metals with other d^n configurations resulted in destabilized products or large activation barriers to N_2 cleavage. For N_2, the same metal is used to bind each end of the molecule. However, for a heteronuclear diatomic molecule, $L_1{\equiv}L_2$, it is reasonable to expect that optimum activation will occur for $M_1 \neq M_2$, where M_1 and M_2 are the metals bound to L_1 and L_2 respectively, as shown in Figure 1. In fact, not only are the metal ions likely to be different, but also their d^n configurations. This greatly increases the possible metal combinations and consequently the number of calculations required to carry out a systematic study to optimize the cleavage reaction with respect to M_1 and M_2. Clearly, a more efficient approach is desirable.

Since the thermodynamic driving force for the cleavage of the small molecule is the formation of very strong M−L bonds in the product, shown in Figure 1, a sensible approach would be to choose metals that show the greatest stabilization of the products. Furthermore, the factors which influence the strength of the M−L bond in the product also affect the degree of activation of the bound small molecule in the intermediate dimer, such as overlap between the metal and L orbitals. Therefore, it seems reasonable that the metal systems which give the strongest $M{-}L_1$ and $M{-}L_2$ bonds will result in the greatest activation of the small molecule, $L_1{\equiv}L_2$, in the intermediate dimer.

This strategy makes the determination of suitable metals considerably easier for two reasons. First, the calculations are computationally less expensive because they are performed on the smaller $LM(NH_2)_3$ fragment, and second, it significantly reduces the number of calculations required because, once the calculations are carried out for L = O, N and C, predictions can be made about any diatomic unit containing these atoms, such as N_2, NO, CO, CN^-, and O_2.

A premise of the above strategy is that the activation barrier associated with the final cleavage step will follow the trends in overall thermodynamics. In principle, there are a number of factors which could affect the validity of this assumption: (i) changes in spin state, particularly for the

(12) Cummins, C. C. *Chem. Commun.* **1998**, No. 17, 1777−1786.
(13) Tsai, Y. C.; Johnson, M. J. A.; Mindiola, D. J.; Cummins, C. C.; Klooster, W. T.; Koetzle, T. F. *J. Am. Chem. Soc.* **1999**, *121*, 10426−10427.
(14) Mindiola, D. J.; Meyer, K.; Cherry, J.-P. F.; Baker, T. A.; Cummins, C. C. *Organometallics* **2000**, *19*, 1622−1624.
(15) Peters, J. C.; Cherry, J. P. F.; Thomas, J. C.; Baraldo, L.; Mindiola, D. J.; Davis, W. M.; Cummins, C. C. *J. Am. Chem. Soc.* **1999**, *121*, 10053−10067.
(16) Tsai, Y. C.; Cummins, C. C. *Inorg. Chim. Acta* **2003**, *345*, 63−69.
(17) Cui, Q.; Musaev, D. G.; Svensson, M.; Sieber, S.; Morokuma, K. *J. Am. Chem. Soc.* **1995**, *117*, 12366−12367.
(18) Neyman, K. M.; Nasluzov, V. A.; Hahn, J.; Landis, C. R.; Rösch, N. *Organometallics* **1997**, *16*, 995−1000.
(19) Hahn, J.; Landis, C. R.; Nasluzov, V. A.; Neyman, K. M.; Rösch, N. *Inorg. Chem.* **1997**, *36*, 3947−3951.
(20) Khoroshun, D. V.; Musaev, D. G.; Morokuma, K. *Organometallics* **1999**, *18*, 5653−5660.
(21) Cherry, J.-P. F.; Johnson, A. R.; Baraldo, L. M.; Tsai, Y.-C.; Cummins, C. C.; Kryatov, S. V.; Rybak-Akimova, E. V.; Capps, K. B.; Hoff, C. D.; Haar, C. M.; Nolan, S. P. *J. Am. Chem. Soc.* **2001**, *123*, 7271−7286.
(22) Christian, G.; Driver, J.; Stranger, R. *Faraday Discuss.* **2003**, *124*, 331−341.

intermediate dimer to product step, (ii) steric effects of the bulky amide groups which are not incorporated in the model calculations reported here, (iii) destabilization of charged intermediate dimer species because of Coulombic repulsion between the metal centers, and (iv) difficulties in synthesizing the "ideal" three-coordinate complexes.

In this paper, the results of a systematic study of the bond energies for the M−N, M−O, and M−C bonds in the L−M(NH$_2$)$_3$ product are presented. The validity of the strategy discussed above is then assessed by comparison of the trend in M−N bond energies with the trend in N$_2$ activation in the model intermediate dimers (H$_2$N)$_3$M−N$_2$−M(NH$_2$)$_3$. If the strategy is sound, then as the N−M(NH$_2$)$_3$ product becomes thermodynamically more stable relative to the reactant M(NH$_2$)$_3$, one should observe increasing N$_2$ activation in the intermediate dimer. Although theoretical studies of nitride bond energies in three-coordinate complexes have been reported,[23,24] our strategy is unique in that is attempts to correlate M−L bond energies with the degree of small molecule activation. Furthermore, a systematic study of the metal dependence of the M−N bond has not been undertaken before.

Computational Details

The calculations carried out in this work were performed using the Amsterdam Density Functional (ADF) program[25−27] (versions 2002.03 and 2004.01) running on either Linux-based Pentium IV computers or the Australian National University Supercomputing Facility. All calculations used the local density approximation (LDA) to the exchange potential, the correlation potential of Vosko, Wilk, and Nusair (VWN),[28] the Becke[29] and Perdew[30] corrections for nonlocal exchange and correlation, and the numerical integration scheme of te Velde and co-workers.[31] Geometry optimizations were performed using the gradient algorithm of Versluis and Ziegler.[32] All-electron triple-ζ Slater-type orbital basis sets (TZP) were used for all atoms. Relativistic effects were incorporated using the zero-order relativistic approximation (ZORA)[33−35] functionality. Minima were confirmed via frequency calculations computed by numerical differentiation of energy gradients in slightly displaced geometries.[36,37] All calculations were carried out in a spin-unrestricted manner. The convergence criteria for the geometry optimizations were 10^{-3} for energy and 10^{-2} for gradient. SCF convergence was set at 10^{-6}. The integration parameter, accint, was set to 4.0 for geometry optimizations and to 6.0 for frequency calculations. Activation barriers for N−N cleavage were obtained from transition-state calculations. The starting geometries for the transition-state searches were estimated from linear transits in which the N−N bond length in the intermediate dimer was incremented while all other geometrical parameters were optimized. Transition states were confirmed via frequency analysis. The M−L bond energies (corrected for zero-point vibrational energy) were analyzed using the bond decomposition scheme available in ADF.[38−40] This analysis involves partitioning the L−M(NH$_2$)$_3$ molecule into two fragments, L and M(NH$_2$)$_3$. The fragments are then brought together in a single-point calculation corresponding to the optimized geometry of the L−M(NH$_2$)$_3$ complex. In this approach, the interaction energy associated with the M−L bonding can be broken down according to the following expression

$$\Delta E = \Delta E_{\mathrm{elstat}} + \Delta E_{\mathrm{Pauli}} + \Delta E_{\mathrm{orb}}$$

where $\Delta E_{\mathrm{elstat}}$ is the electrostatic interaction between the two fragments, $\Delta E_{\mathrm{Pauli}}$ is the four-electron two-orbital repulsive term, and ΔE_{orb} is the orbital interaction term which can be further partitioned into contributions from each of the irreducible representations of the molecular point group.

Results and Discussion

To determine the bond energies for the M−N, M−O, and M−C bonds in the L−M(NH$_2$)$_3$ product, it is necessary to calculate the lowest-energy structures of both the M(NH$_2$)$_3$ reactant and L−M(NH$_2$)$_3$ product fragments. The results of geometry optimizations on these fragment molecules are detailed in Tables 1−4 and Figures 2 and 4.

1. M(NH$_2$)$_3$ Reactant. An earlier computational study[41] using extended Hückel and DFT calculations gave a number of worthwhile insights into trends in the structure and spin state of first-row ML$_3$ complexes. These calculations predicted high-spin complexes for d^1−d^6 metal configurations. Our study also examines 1st-row complexes but extends the work to include 2nd- and 3rd-row transition metals and structures possessing both trigonal (D_{3h}, C_3) and nontrigonal (C_s, C_1) symmetries. Given the size of the bulky N(R)Ar amide ligands used in the experimental complexes, it is sensible to restrict the calculations to structures possessing a trigonal or pseudotrigonal arrangement of the N(R)Ar ligands around the metal. However, our recent work[42] has shown that rotation of one or more of these bulky ligands is possible, even in the N$_2$-bridged dimer. This is born out experimentally in the reported crystal structure for the [Ar(^{t}Bu)N]$_3$Mo−(μ-N$_2$)−Nb[N(^{i}Pr)Ar]$_3$ dimer which exhibits rotation of the N(^{i}Pr)Ar ligands on the Nb center.[14] The spin state, symmetry, M−N$_{\mathrm{amide}}$ bond lengths, and structure type calculated for the lowest-energy structures of M(NH$_2$)$_3$

(23) Pandey, K. K.; Frenking, G. *Eur. J. Inorg. Chem.* **2004**, 4388−4395.
(24) Vyboishchikov, S. F.; Frenking, G. *Theor. Chem/Acc.* **1999**, *102*, 300−308.
(25) te Velde, G.; Bickelhaupt, F. M.; Baerends, E. J.; Fonseca Guerra, C.; Van Gisbergen, S. J. A.; Snijders, J. G.; Ziegler, T. *J. Comput. Chem.* **2001**, *22*, 931−967.
(26) Fonseca Guerra, C.; Snijders, J. G.; Te Velde, G.; Baerends, E. J. *Theor. Chem. Acc.* **1998**, *99* (6), 391−403.
(27) *Amsterdam Density Functional*; Scientific Computing & Modelling: Amsterdam, The Netherlands, 2002.
(28) Vosko, S. H.; Wilk, L.; Nusair, M. *Can. J. Phys.* **1980**, *58* (8), 1200−1211.
(29) Becke, A. D. *Phys. Rev. A* **1988**, *38* (6), 3098−3100.
(30) Perdew, J. P. *Phys. Rev. B* **1986**, *33* (12), 8822−8824.
(31) Velde, G. T.; Baerends, E. J. *J. Comput. Phys.* **1992**, *99* (1), 84−98.
(32) Versluis, L.; Ziegler, T. *J. Chem. Phys.* **1988**, *88* (1), 322−328.
(33) van Lenthe, E.; Baerends, E. J.; Snijders, J. G. *J. Chem. Phys.* **1993**, *99* (6), 4597−4610.
(34) van Lenthe, E.; Baerends, E. J.; Snijders, J. G. *J. Chem. Phys.* **1994**, *101* (11), 9783−9792.
(35) van Lenthe, E.; Ehlers, A.; Baerends, E. J. *J. Chem. Phys.* **1999**, *110* (18), 8943−8953.
(36) Fan, L. Y.; Ziegler, T. *J. Phys. Chem.* **1992**, *96* (17), 6937−6941.
(37) Fan, L. Y.; Ziegler, T. *J. Chem. Phys.* **1992**, *96* (12), 9005−9012.
(38) Bickelhaupt, F. M.; Baerends, E. J. In *Reviews in Computational Chemistry*; Wiley: New York, 2000; Vol. 15, pp 1−86.
(39) Ziegler, T.; Rauk, A. *Inorg. Chem.* **1979**, *18* (6), 1558−1565.
(40) Ziegler, T.; Rauk, A. *Inorg. Chem.* **1979**, *18* (7), 1755−1759.
(41) Palacios, A. A.; Alemany, P.; Alvarez, S. *Inorg. Chem.* **1999**, *38* (4), 707−715.
(42) Christian, G.; Stranger, R.; Yates, B. F.; Graham, D. C. *Dalton Trans.* **2005** (5), 962−968.

Table 1. Symmetry, Spin State, and Structural Data for d^1-d^6 $M(NH_2)_3$ Complexes

	metals	spin	structure		M−N$_{amide}$ calcd	M−N$_{amide}$ exptl	compound
d^1	Ti^{III}	1/2	**B**	$\sim D_{3h}$	1.916	1.933, 1.992, 2.005	$Ti[N(R)Ar]_3$[48] ^{g}
	Zr^{III}	1/2	**B**	C_3	2.054		
	Hf^{III}	1/2	**B**	C_3	2.024		
d^2	Ti^{II}	0	**E**	$C_s{}^a$	1.945, 1.935		
	Zr^{II}	0	**E**	$C_s{}^a$	2.082, 2.079		
	Hf^{II}	0	**E**	$\sim C_s{}^a$	2.056, 2.057, 2.058		
	V^{III}	1	**E**	$\sim C_s$	1.871, 1.882	1.945, 1.905, 1.900	$V[N(Ad)Ar]_3$[49]
	Nb^{III}	1	**G**	C_s	1.999, 2.013		
	Ta^{III}	0	**F**	C_s	1.951, 1.959		
	Cr^{IV}	1	**E**	$\sim C_s$	1.791, 1.795, 1.796		
	Mo^{IV}	1	**G**	$\sim C_s$	1.905, 1.921, 1.922		
	W^{IV}	1	**G**	C_s	1.897, 1.916		
d^3	V^{II}	3/2	**C**	C_1 ($\sim C_3$)	1.957		
	Nb^{II}	3/2	**A**	D_{3h}	2.089		
	Ta^{II}	1/2	**D**	C_s	2.012, 2.016		
	Cr^{III}	3/2	**C**	C_3	1.854	1.854, 1.875, 1.864	$Cr[N(R)Ar]_3$[50] ^{g}
	Mo^{III}	3/2	**A**	D_{3h}	1.982	1.960, 1.964, 1.977	$Mo[N(R)Ar]_3$[5] ^{g}
	W^{III}	3/2	**A**	D_{3h}	1.971		
	Mn^{IV}	3/2	**C**	$\sim C_3{}^b$	1.787		
	Tc^{IV}	1/2	**E**	C_s	1.867, 1.882		
	Re^{IV}	$3/2^e$	**C**	C_1	1.907, 1.905, 1.900		
d^4	Cr^{II}	2	**F**	$C_s{}^a$	1.958, 1.994		
	Mo^{II}	1	**C**	$C_3{}^a$	2.004		
	W^{II}	1	**A**	D_{3h}	1.984		
	Mn^{III}	2	**F**	$\sim C_s{}^a$	1.871, 1.868	1.890	hs d^4 $Mn\{N(SiMe_3)_2\}_3$[51]
	Tc^{III}	1	**C**	$\sim C_3{}^b$	1.944, 1.929		
	Re^{III}	1	**A**	D_{3h}	1.916		
	Fe^{IV}	1	**D**	$C_1{}^d$	1.738, 1.739, 1.774		
	Ru^{IV}	0	**E**	$\sim C_s$	1.850, 1.851, 1.863		
	Os^{IV}	0	**E**	$\sim C_s$	1.845, 1.853		
d^5	Fe^{III}	5/2	**B**	C_3	1.871	1.917	$Fe\{N(SiMe_3)_2\}_3$[52]
	Ru^{III}	1/2	**A**	D_{3h}	1.897		
	Os^{III}	1/2	**A**	D_{3h}	1.903		
d^6	Co^{III}	1	**E**	$\sim C_s{}^a$	1.801, 1.795	1.870	hs d^6 $Co\{N(SiMe_3)_2\}_3$[51]
	Rh^{III}	0	**A**	D_{3h}	1.865		
	Ir^{III}	0	**A**	D_{3h}	1.867		

^{a} M−NH_2 is not planar. ^{b} Ligands tilted at different angles. ^{c} One ligand tilted ∼25°. ^{d} Ligand tilted 72°. ^{e} Spin doublet very close in energy. ^{f} One ligand upright. ^{g} R =$C(CD_3)_2Me$.

complexes with M = M^{III} (d^1-d^6), M^{II} (d^2-d^4), and M^{IV} (d^3-d^5) are summarized in Table 1, along with the experimental M−N$_{amide}$ bond lengths where available. The calculated geometries correspond to seven basic structure types which are designated A−G in Figure 2.

For the first-row transition metals, high-spin complexes are predicted, in agreement with the above study, except for Co^{III} where a triplet ground state is calculated. For the second- and third-row transition metals, lower-spin states are favored. The change in spin state can be explained by the increasing gap between the $9a_1'$ and $3e''$ levels shown in Figure 3. This results from the increasingly antibonding nature of the d_{xz} and d_{yz} orbitals down a group, which are destabilized relative to the essentially nonbonding d_{z^2} orbital. Furthermore, as the group is descended, the greater radial dilation of the d orbitals results in lower spin-pairing energies. Both effects favor low-spin states.

The calculated structures can also be rationalized on the basis of the molecular orbital diagram in Figure 3. For d^3 complexes, the lowest-energy doublet has only one electron in the degenerate $3e''$ MO and therefore is subject to a Jahn−Teller distortion to give structures D or E in Figure 2. Similar Jahn−Teller distorted geometries are observed in the calculated structures for the d^2 and d^4 $M(NH_2)_3$ complexes in Table 1 when either the $3e''$ or $9e'$ levels are occupied by an odd number of electrons. For d^1 complexes, the single d electron occupies the nonbonding d_{z^2} orbital, and so the orientation of the ligands would not be expected to affect its energy significantly. However, as has been explained in the previous study of ML_3 complexes,[41] the nonbonding $1a_2'$ level favors a coplanar ligand orientation and as a result, the d^1 complexes adopt this ligand arrangement.

2. L−M(NH_2)$_3$ Product. Calculations were carried out on L−M(NH_2)$_3$ complexes with M = M^{II}, M^{III}, and M^{IV} and L = N, O, and C. The results are summarized in Table 2 for L = N with d^2-d^6 metal configurations, in Table 3 for L = O with d^1-d^3 metal configurations, and Table 4 for L = C with d^3-d^5 metal configurations. The spin state, symmetry, M−L and M−N$_{amide}$ bond lengths, and structure type calculated for the lowest-energy L−M(NH_2)$_3$ structures are also summarized in Tables 2−4, along with the experimental M−L and M−N$_{amide}$ bond lengths where available. The calculated geometries correspond to the five basic structure types designated **1**−**5** in Figure 2.

The MO diagram for N−Mo(NH_2)$_3$ is shown in Figure 4. The ground-state structure for this complex has C_{3v} symmetry and is a spin singlet because the $15a_1$ HOMO and 10e HOMO−1 levels fully occupied. All the L−M(NH_2)$_3$

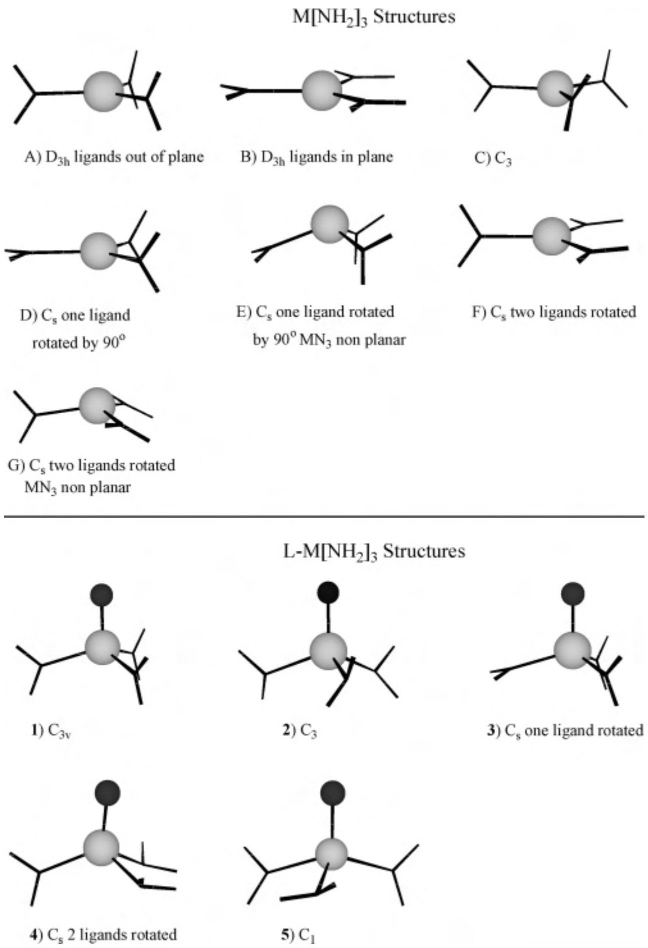

Figure 2. Geometries for M(NH$_2$)$_3$ and L−M(NH$_2$)$_3$ complexes.

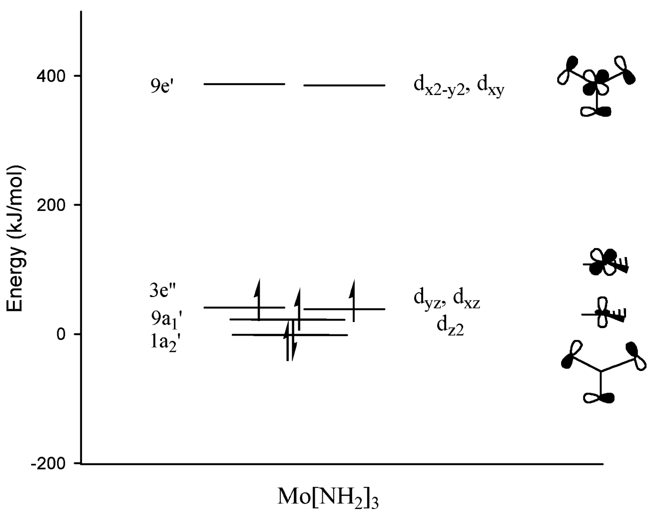

Figure 3. Simplified orbital diagram for Mo^{III}(NH$_2$)$_3$.

complexes investigated are low spin with either spin-singlet or spin-doublet ground states. Regardless of the nature of L, isoelectronic complexes are calculated to have very similar structures. For example, all O−M(NH$_2$)$_3$, N−M(NH$_2$)$_3$, and C−M(NH$_2$)$_3$ complexes containing d^2, d^3, and d^4 metal ions, respectively, have C_{3v} or C_3 structures. Lower-symmetry structures result when the 10e level is singly or triply occupied because of Jahn−Teller distortions.

3. (H$_2$N)$_3$M−L Bond Energies. To determine the optimum metal and d^n configuration for activating small molecules such as N$_2$, NO, CO, and CN$^-$, the M−L bond energies in the L−M(NH$_2$)$_3$ complexes were calculated for L = N, O, and C using the equation

$$E_{\text{bond}} = E[\text{LM(NH}_2)_3] - E[\text{L}] - E[\text{M(NH}_2)_3]$$

where E[M(NH$_2$)$_3$], E[LM(NH$_2$)$_3$], and E[L] are the energies of the reactant, product, and L fragment, respectively. The calculated M−N, M−O, and M−C bond energies are given in Table 5 and Table 6.

Solution calorimetry has been used to obtain experimental Mo−O and Mo−N bond dissociation enthalpies for N−Mo-[N(R)Ar]$_3$ and O−Mo[N(R)Ar]$_3$ complexes.[8,21] The calculated Mo−N bond energy of 638 kJ mol^{-1} is in very good agreement with experimental value of 649.8 ± 13.8 kJ mol^{-1}. The corresponding Mo−N bond energy obtained from the QM/MM calculations on the full Mo[N(R)Ar]$_3$ system is approximately 20 kJ mol^{-1} smaller.[43] This decrease can be rationalized on the basis of the steric crowding being greater in the product than in the reactant, which in turn reduces the Mo−N bond strength. The calculated M−O value of 684 kJ mol^{-1} is in reasonable agreement with the measured value of 651.0 ± 6.7 kJ mol^{-1} considering the differences between the real and model systems. The steric bulk of the real N(R)-Ar ligands may not allow the system to adopt the C_1 geometry calculated for the model O−Mo(NH$_2$)$_3$ complex. If O−Mo(NH$_2$)$_3$ is constrained to C_3 symmetry, the calculated Mo−O bond energy is reduced to 648 kJ mol^{-1} which is well within the error range of the experimental value.

The M−N, M−O, and M−C bond energies for L−M(NH$_2$)$_3$ involving second-row M^{III} ions with d^1−d^6 configurations are summarized in Table 5. The M−N bond strength increases from d^2 to d^3 metals and then progressively decreases from d^4 to d^6 metals. Similar trends are also observed for first- and third-row metals. Thus, along any transition series, the maximum M−N bond strength occurs for d^3 metals. The reason for this trend becomes evident from the molecular orbital diagram for N−Mo(NH$_2$)$_3$ shown in Figure 4. The three metal-based d electrons are able to combine with the three p electrons on nitrogen to form a Mo−N triple bond. For d^n configurations with n > 3, electrons are forced to occupy a metal−nitrogen antibonding orbital, whereas for n < 3, electrons are removed from a metal−nitrogen bonding orbital. Both situations result in weaker metal−nitrogen bonding compared to d^3 metals.

Similar trends are observed in the M−O and M−C bond energies shown in Table 5. The metal−oxygen bonds are strongest for d^2 metals, and the metal−carbon bonds are strongest for d^4 metals. These trends are consistent with the fact that d^2 and d^4 metal configurations provide the necessary number of electrons to occupy all three M−L bonding orbitals in the O−M(NH$_2$)$_3$ and C−M(NH$_2$)$_3$ complexes, respectively. Thus, in principle, M−O and M−C triple bonds

(43) Christian, G.; Stranger, R. Unpublished data.

Table 2. Symmetry, Spin State, and Structural Data for N−M(NH$_2$)$_3$ Complexes

	metals	spin	structure		calculated M−N	calculated M−NH$_2$	experimental M−N	experimental M−NH$_2$	compound
d^2	Nb^{III}	1/2	**3**	C_s	1.787	2.059, 2.017			
	Ta^{III}	1/2	**3**	C_s	1.804	2.018, 1.997			
	V^{II}	0	**2**	C_3	1.590	1.947			
	Nb^{II}	0	**1**	C_{3v}	1.725	2.089			
	Ta^{II}	0	**1**	C_{3v}	1.737	2.061			
	Cr^{III}	0	**1**	C_{3v}	1.534	1.836	1.544	1.844, 1.842, 1.840	NCr[N^{i}Pr$_2$]$_3$[53]
d^3	Mo^{III}	0	**1**	C_{3v}	1.664	1.978	1.658	1.979	NMo[N(^{t}Bu)Ph]$_3$[4]
	W^{III}	0	**1**	C_{3v}	1.684	1.968			
	Mn^{IV}	0	**1**	C_{3v}	1.506	1.780			
	Tc^{IV}	0	**1**	C_{3v}	1.633	1.914			
	Re^{IV}	0	**1**	C_{3v}	1.654	1.909			
d^4	Tc^{III}	1/2	**5**	C_1	1.653	1.962, 1.971, 1.994			
	Re^{III}	1/2	**5**	C_1	1.676	1.947, 1.965, 1.986			
d^5	Ru^{III}	0	**4**	$\sim C_s$	1.643	1.951, 1.959, 1.961			
	Os^{III}	0	**4**	C_s	1.666	1.938, 1.960			
d^6	Rh^{III}	1/2	**3**	$\sim C_s$	1.665	1.976, 1.978, 2.004			
	Ir^{III}	1/2	**3**	$\sim C_s$	1.676	1.959, 1.963, 2.024			

Table 3. Symmetry, Spin State, and Structural Data for O−M(NH$_2$)$_3$ Complexes

	metals	spin	symmetry		calculated M−O	calculated M−NH$_2$	experimental M−O	experimental M−NH$_2$	compound
d^1	Zr^{III}	1/2	**1**	C_s ($\sim C_{3v}$)	1.780	2.173			
	Hf^{III}	1/2	**4**	$\sim C_s{}^a$	1.799	2.101, 2.117, 2.119			
	Ti^{II}	0	**2**	$\sim C_3$	1.677	2.010			
	Zr^{II}	0	**2**	C_3	1.816	2.166			
	Hf^{II}	0	**2**	C_3	1.813	2.124			
	V^{III}	0	**2**	$\sim C_3$	1.597	1.866, 1.867, 1.869			
d^2	Nb^{III}	0	**2**	C_3	1.729	2.016			
	Ta^{III}	0	**2**	C_3	1.737	1.998			
	Cr^{IV}	0	**2**	C_3	1.554	1.788			
	Mo^{IV}	0	**2**	C_3	1.683	1.926			
	W^{IV}	0	**2**	$\sim C_3$	1.693	1.919			
d^3	Mo^{III}	1/2	**5**	C_1	1.722	1.973, 1.974, 1.978	1.706	1.973, 1.980, 1.990	O−Mo[N(R)Ar]$_3$[8], R = C(CD$_3$)$_2$Me
	W^{III}	1/2	**4)**	C$_s$	1.728	1.963, 1.971			

^{a} Tilted ∼20° (close to C_3).

Table 4. Symmetry, Spin State, and Structural Data for C−M(NH$_2$)$_3$ Complexes

	metals	spin	symmetry		calculated M−C	calculated M−NH$_2$	experimental M−C	experimental M−NH$_2$	compound
d^3	Mo^{III}	1/2	**3**	$\sim C_s$	1.760	2.015, 1.966			
	W^{III}	1/2	**3**	C_s	1.785	1.986, 1.958			
d^4	Cr^{II}	0	**2**	C_3	1.603	1.886			
	Mo^{II}	0	**1**	C_{3v}	1.733	2.028	1.713	2.008, 2.010, 2.013	[C−Mo{N(R)Ar}$_3$]$^-$, R = C(CD$_3$)$_2$Me [6]
	W^{II}	0	**1**	C_{3v}	1.758	2.010			
	Mn^{III}	0	**1**	C_{3v}	1.571	1.805			
	Tc^{III}	0	**1**	C_{3v}	1.694	1.944			
	Re^{III}	0	**1**	C_{3v}	1.721	1.937			
	Fe^{IV}	0	**1**	C_{3v}	1.567	1.762			
	Ru^{IV}	0	**1**	C_{3v}	1.688	1.900			
	Os^{IV}	0	**1**	C_{3v}	1.709	1.898			
d^5	Ru^{III}	1/2	**3**	C$_s$	1.677	2.017, 1.972			
	Os^{III}	1/2	**5**	C$_1$	1.709	1.942, 1.969, 1.999			

are possible if d^2 and d^4 metals are used. This point is discussed in more detail for the bond energy analysis.

In addition to the metal d^n configuration, the M−L bond strength in the product is also dependent on the charge on the metal and its position within a group. Their effect on the bond energies can be appreciated from the data summarized in Table 6 where the optimum metal configurations of d^2, d^3, and d^4 have been used in the calculation of the M−O, M−N, and M−C bond energies, respectively. The M^{II}−O, M^{III}−N, and M^{IV}−C bond energies increase both down a group and to the left of a period. These trends correlate with increasing d orbital size on the metal, resulting in enhanced overlap with the σ and π orbitals on L and thus a stronger M−L bond.[44]

The results of the bond-energy decomposition for selected L−M(NH$_2$)$_3$ complexes is given in Table 7. In all cases, the orbital contribution to the bonding is larger than the electrostatic contribution, indicating a strongly covalent bond.

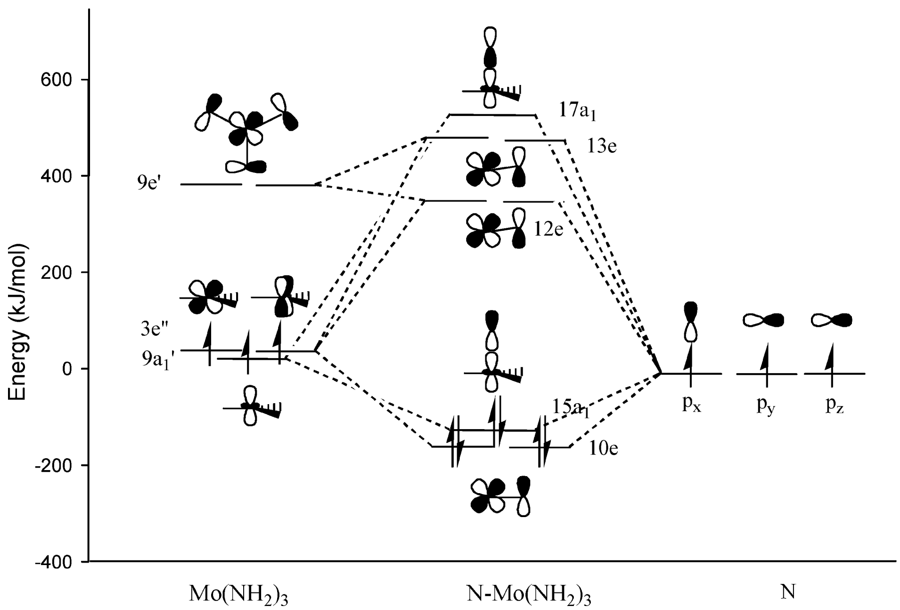

Figure 4. Simplified molecular orbital diagram for N−Mo(NH$_2$)$_3$ with C_{3v} symmetry.

Table 5. M−L Bond Energies (kJ mol^{-1}) in L−M^{III}(NH$_2$)$_3$ Complexes, for L = N, O, and C

	Zr^{III} (d^1)	Nb^{III} (d^2)	Mo^{III} (d^3)	Tc^{III} (d^4)	Ru^{III} (d^5)	Rh^{III} (d^6)
M−N		−470	−638[a]	−547	−437	−256
M−O	−547	−813	−684			
M−C			−526	−694	−531	

[a] −649.8 ± 13.8 kJ mol^{-1} for experimental Mo−N bond energy in N−Mo[N(R)Ar]$_3$.[21]

Table 6. M−L Bond Energies (kJ mol^{-1}) in L−M(NH$_2$)$_3$ Complexes for L = N, O, and C

M−N		M−O		M−C	
d^3 metals	energy	d^2 metals	energy	d^4 metals	energy
V^{II}	−635	Ti^{II}	−833	Cr^{II}	−592
Nb^{II}	−713	Zr^{II}	−824	Mo^{II}	−722
Ta^{II}	−735	Hf^{II}	−828	W^{II}	−747
Cr^{III}	−500	V^{III}	−721	Mn^{III}	−515
Mo^{III}	−638[a]	Nb^{III}	−813	Tc^{III}	−694
W^{III}	−717	Ta^{III}	−865	Re^{III}	−733
Mn^{IV}	−411	Cr^{IV}	−579	Fe^{IV}	−497
Tc^{IV}	−574	Mo^{IV}	−699[a]	Ru^{IV}	−603
Re^{IV}	−663	W^{IV}	−784	Os^{IV}	−681

[a] Experimental values for Mo−N and Mo−O bond energies in N−Mo-[N(R)Ar]$_3$ and O−Mo[N(R)Ar]$_3$ complexes are −649.8 ± 13.8 and −651.0 ± 6.7 kJ mol^{-1}, respectively.[21,8]

However, the ratio of the orbital to electrostatic contribution decreases down a group, indicating that the M−N bond becomes less covalent as the group is descended. From W^{III} to Ta^{II}, there is a large jump in the Pauli, electrostatic, and orbital contributions. This is partly the result of changes in the ground state of the fragments because Ta^{II}(NH$_2$)$_3$ is a spin doublet, while the W^{III} and Re^{IV} complexes are spin quartets. The contributions calculated using a quartet Ta(NH$_2$)$_3$ fragment are closer to the values for W^{III} and Re^{IV}.

(44) One exception is the Ti^{II}−O bond energy which is slightly greater than both the Zr^{II}−O and Hf^{II}−O bond energies. However, all three values differ only by approximately 10 kJ mol^{-1}, and this small energy span is consistent with the observation that the range of bond energies within a group decreases markedly as the metal charge changes from +4 to +2.

Since C_{3v} symmetry was used for all L−M(NH$_2$)$_3$ complexes in this analysis, the orbital contribution to the M−L bond energy can be further decomposed into contributions from each of the C_{3v} irreducible representations as follows:

$$\Delta E_{\mathrm{orb}} = \Delta E_{\mathrm{A1}} + \Delta E_{\mathrm{A2}} + \Delta E_{\mathrm{E}}$$

The A$_1$ contribution comes from the M−L σ bonding, whereas the E contribution relates to the M−L π bonding. The A$_2$ contribution should be negligible because there is no M−L bond of this symmetry. The results in Table 7 show that the A$_1$ and E contributions are similar for all the M−N bonds. Since the E contribution is the sum of both M−L π bonds, then each M−L π bond is approximately half the strength of the M−L σ bond, and this is consistent with strong M−N triple bonds.

The M−O, M−N, and M−C bonds in third-row L−M^{III}(NH$_2$)$_3$ (M^{III} = Ta, W, Re) complexes are also compared in Table 7. In all cases, the orbital contribution is larger than the electrostatic contribution indicating predominantly covalent bonding, with the Re^{III}−C bond having the highest ratio of $\Delta E_{\mathrm{elstat}}$ to ΔE_{orb} and therefore being the least covalent of the bonds analyzed. Further examination of the orbital interaction reveals that the A$_1$(σ) contribution does not vary greatly as L changes, but the E(π) contribution increases significantly; for the Re^{III}−C and Ta^{III}−O bonds, the overall π contribution is actually larger than the σ contribution. This description of the bonding is consistent with Ta^{III}−O and Re^{III}−C triple bonds, as predicted from the MO analysis on the basis of all three M−L-bonding MOs being fully occupied. Furthermore, since the bonding energies in Table 7 are in the order W^{III}−N < Re^{III}−C < Ta^{III}−O, then both the Ta−O and Re−C bonds, in particular, the latter, are stronger than the W^{III}−N bond.

In principle, the bond-energy results can guide the choice of metals for binding or activating small molecules such as N$_2$, NO, CO, and CN$^-$. The data in Table 6 indicate that the strongest metal−nitride bonds occur for Ta^{II}, W^{III}, and Nb^{II},

Table 7. Bonding Energy Decomposition for the L−M Bond (L = N, C, and O) in L−M$(NH_2)_3$ Complexes with C_{3v} Symmetry

				ΔE_{orb} (eV)					
L	metal	ΔE_{Pauli} (eV)	ΔE_{elstat} (eV)	A_1 (σ)	A_2 (nb)	E (π)	total	BE (eV)	BE_{corr} (eV)[b]
	Cr^{III}	16.0468	−8.3335	−6.9455	0.0020	−6.8380	−13.7816	−6.0683	−5.3644
N	Mo^{III}	18.1979	−9.8184	−8.1514	0.0014	−7.5693	−15.7193	−7.3399	−6.8006
	W^{III}	19.6962	−11.2716	−8.5517	0.0013	−8.0488	−16.5993	−8.1748	−7.6037
	Ta^{II} (d)[a]	26.0029	−13.9518	−13.8178	0.0017	−6.8214	−20.6375	−8.5865	−7.7655
N	W^{III}	19.6962	−11.2716	−8.5517	0.0013	−8.0488	−16.5993	−8.1748	−7.6037
	Re^{IV}	19.2946	−10.8863	−8.0313	0.0012	−7.8866	−15.9167	−7.5086	−7.0621
O	Ta^{III}	27.4150	−14.0518	−9.6278	0.0021	−13.5394	−23.1652	−9.8019	−9.1079
N	W^{III}	19.6962	−11.2716	−8.5517	0.0013	−8.0488	−16.5993	−8.1748	−7.6037
C	Re^{III}	26.6743	−15.4017	−8.7433	0.0033	−10.7110	−19.4509	−8.1783	−7.8312

[a] Using a quartet $Ta^{II}(NH_2)_3$ fragment: Pauli = 17.2595 eV, electrostatic = −9.7853 eV, A_1 = −8.1676 eV, A_2= 0.0003 eV, E= −8.0628 eV, total orbital contribution= −16.2301 eV, BE= −8.7560 eV, and BE_{corr}= −8.2448 eV. [b] Because of technical requirements, the fragments must be spin-restricted and the M$(NH_2)_3$ fragments are distorted from their optimal geometry as the atom positions correspond to those for the optimized L−M$(NH_2)_3$ complexes. The BE_{corr} is adjusted for both these effects. The BE values do not include zero-point energy corrections.

Table 8. Spin State and N−N Bond Length in the Intermediate Dimer, Activation Energy for N_2 Cleavage (E_a), and the M−N Bond Energy for the d^3 M$(NH_2)_3$ Systems

metal	spin	N−N (Å)	E_a (kJ mol^{-1})	E_s (kJ mol^{-1})	M−N bond energy (kJ mol^{-1})
V^{II}	1	1.270	133	−331	−635
Nb^{II}	1	1.269	56	−476	−713
Ta^{II}	1	1.298	88	−521	−735
Cr^{III}	1	1.196	140	−58[b]	−500
Mo^{III}	0	1.221	59	−335	−638
W^{III}	1	1.278	34	−491	−717
Mn^{IV}	1	1.164	241	118[c]	−411
Tc^{IV}	0	1.194	172	−191	−574
Re^{IV}	0	1.211	102	−386	−663

[a] The value in parentheses is the activation barrier (E_a) calculated for the singlet state. [b] N−N cleavage step is endothermic. [c] Both the intermediate dimer and products are destabilized relative to the reactants.

the strongest metal−oxide bonds for Ta^{III}, Zr^{II}, and Nb^{III}, and the strongest metal−carbide bonds for W^{II}, Re^{III}, and Mo^{II}.

4. N−N Activation. On the basis of the M−N bond energies reported in Table 6, the best activation of dinitrogen in $(H_2N)_3$M−N_2−M$(NH_2)_3$ dimers should occur for d^3 metals, in particular, when M = Ta^{II}, W^{III} or Nb^{II}. The accuracy of this prediction can be assessed by comparing the M−N bond energies with the calculated N−N bond lengths in the intermediate dimer. If the strategy outlined earlier is valid, then the calculated N−N bond distance should lengthen as the M−N bond strength increases. Indeed, from the calculated values for the d^3 metals in Table 8, it is apparent that the strategy does hold in that the calculated N−N bond lengths follow the same trends observed for the M−N bond energies, increasing down a group and to the left of a period.

Unfortunately, the N−N bond length is not always a reliable measure of the ease of N_2 bond cleavage as the activation barrier to cleavage may still be large. For instance, although the $Mo^{III}Nb^{III}$ dimer (Ar[^{t}Bu]N)$_3$Mo(μ-N_2)Nb-(N[^{i}Pr]Ar)$_3$ has a significantly activated dinitrogen bond (ca. 1.235 Å), N−N bond cleavage is unfavorable because it does not have the required number of electrons to reductively cleave the N−N bond.[45] Included in Table 8 are the calculated activation barriers (E_a) for cleavage of the N−N bond in the intermediate dimers involving d^3 metal ions. With the exception of Ta^{II}, there is a clear trend in that the activation barriers decrease both down a group and to the left of a period as the M−N bond strength increases.

The values reported in Table 8 do not include the steric effects of the N(R)Ar ligands. Our calculations on the full Mo[N(R)Ar]$_3$ system indicate that the steric bulk of the ligands increases the activation barrier for N−N cleavage by approximately 30 kJ mol^{-1}.[43] Both changes in spin state and steric bulk have been shown to influence the deoxygenation of (silox)$_3$WNO by M(silox)$_3$ (M = V, Nb, or Ta).[46]

A further complication occurs for the V^{II} and Mn^{IV} triads in that the intermediate dimer has two charged metal centers resulting in Coulombic repulsion and hence destabilization of the intermediate dimer and transition-state species. Consequently, the calculated activation barriers are likely to be different from those measured in solution where Coulombic effects are diminished.

Conclusion

On the basis of the calculated L−M bond energies in L−M$(NH_2)_3$ (L = N, O and C) complexes, the metals most suited for activating and cleaving N_2 are the d^3 metals Ta^{II}, W^{III}, and Nb^{II}. In principle, all three metals should result in a more exothermic cleavage reaction than the experimentally known Mo^{III} system but the lower charge on Ta^{II} and Nb^{II} will result in an intermediate dimer which is anionic, and this may present problems experimentally. For NO, CO, and CN^- cleavage, a heterometallic dimer is required to optimize the binding of the bridging diatomic. For NO, a d^3d^2 dimer with W^{III} bound to N and Ta^{III} bound to O gives the best thermodynamics for a neutral dimer, but in fact, our preliminary investigations indicate that a Mo^{III}−V^{III} dimer, with V^{III} bound to O, is quite capable of cleaving the NO bond.[43] Presumably, this is a consequence of the NO bond being significantly weaker than the triple bond in N_2. Again, choosing an overall neutral system, a d^3d^3 dimer with W^{III} bound to N and Re^{IV} bound to C is predicted to optimize the cleavage of CN^-. The d^3d^3 metal dimer configuration for CN^-, rather than a d^4d^3 configuration, arises because the

(45) Christian, G.; Stranger, R. *Dalton Trans.* **2004**, No. 16, 2492−2495.

(46) Veige, A. S.; Slaughter, L. M.; Lobkovsky, E. B.; Wolczanski, P. T.; Matsunaga, N.; Decker, S. A.; Cundari, T. R. *Inorg. Chem.* **2003**, *42* (20), 6204−6224.

negative charge on the cyanide ion makes it isoelectronic with N_2. In the case of CO, the bond-energy calculations indicate that that the neutral d^4d^2 metal dimer, with Re^{III} bound to C and Ta^{III} bound to O, is thermodynamically best suited for cleaving CO.

Although the above choice of metals optimize the exothermic nature of the cleavage reactions, it is necessary to examine the whole reaction profile, including activation barriers, to determine whether cleavage is favorable. Furthermore, it may not be possible to synthesize the most suitable three-coordinate complex on thermodynamic grounds. For example, although earlier calculations[17,22] have shown that W[N(R)Ar]$_3$ is more favorable for N_2 activation than Mo[N(R)Ar]$_3$, the W^{III} complex has yet to be isolated experimentally. Like the Nb^{III} analogue, this species may be susceptible to intramolecular rearrangement or decomposition reactions.[47] In such cases, other ligand systems such as M(silox)$_3$ may be suitable alternatives. Even taking these problems into consideration, our results for N_2 cleavage show a clear correlation between calculated M−N bond energies and N_2 activation in thee-coordinate complexes. Consequently, we intend to extend this study to investigate the cleavage reactions of NO, CO, and CN^- by M[N(R)Ar]$_3$ complexes.

Acknowledgment. The authors greatly thank the Australian Research Council for financial support in the form of an Australian Postgraduate Award for G.C. and a Discovery Project Grant for R.S. and B.F.Y. The Australian National University is also acknowledged for funding of this project through the Faculty Research Grant Scheme.

Supporting Information Available: Optimized structures and energies of M(NH$_2$)$_3$ and L−M(NH$_2$)$_3$ complexes, where L = N, C, and O. This material is available free of charge via the Internet at http://pubs.acs.org.

IC051778U

(47) Figueroa, J. S.; Cummins, C. C. *J. Am. Chem. Soc.* **2003**, *125* (14), 4020−4021.
(48) Wanandi, P. W.; Davis, W. M.; Cummins, C. C.; Russell, M. A.; Wilcox, D. E. *J. Am. Chem. Soc.* **1995**, *117* (7), 2110−2111.
(49) Ruppa, K. B. P.; Desmangles, N.; Gambarotta, S.; Yap, G.; Rheingold, A. L. *Inorg. Chem.* **1997**, *36* (6), 1194−1197.
(50) Cummins, C. C. *Progress in Inorganic Chemistry,* **1998**, *47*, 685−836.
(51) Ellison, J. J.; Power, P. P.; Shoner, S. C. *J. Am. Chem. Soc.* **1989**, *111* (20), 8044−8046.
(52) Hursthouse, M. B.; Rodesiler, P. F. *J. Chem. Soc., Dalton Trans.* **1972** (19), 2100−2102.
(53) Odom, A. L.; Cummins, C. C.; Protasiewicz, J. D. *J. Am. Chem. Soc.* **1995**, *117* (24), 6613−6614.